Materiales de Construcción
Vol. 73, Issue 351, July-September 2023, e322
ISSN-L: 0465-2746
https://doi.org/10.3989/mc.2023.325822

Analysis of two experimental setups to study mode II fracture on fibre-reinforced gypsum notched specimens

F. Suárez ✉, J.F. Aceituno, J. Donaire-Ávila

Departamento de Ingeniería Mecánica y Minera. Universidad de Jaén. Campus Científico-Tecnológico de Linares, (Jaén, Spain)
✉: fsuarez@ujaen.es

Received 9 November 2022
Accepted 17 February 2023
Available on line 28 Agosto 2023

ABSTRACT: The main aim of this work is to study two relevant experimental setups designed for studying shear fracture and see if any of them allows studying the evolution of fracture under Mode II conditions, not only inducing a shear stress state at the onset of fracture. Two tests have been selected, a standardised test described by a Japanese standard, here referred to as the JSCE test, and the push-off test. These tests have been carried out on fibre-reinforced gypsum specimens with increasing proportions of polypropylene fibres and monitored by means of digital image correlation (DIC). The results show that fracture under Mode II conditions is relatively easy to induce with both tests, but once fracture begins, it is extremely difficult to induce a fracture process under Mode II. In general, Mode II has an important role at the onset on fracture, but Mode I predominates afterwards.

KEY WORDS: Mode II; Shear; Push-off test; Digital image correlation; Fibre-reinforced gypsum.

Citation/Citar como: Suárez, F.; Aceituno, J.F.; Donaire-Ávila, J. (2023) Analysis of two experimental setups to study mode II fracture on fibre-reinforced gypsum notched specimens. Mater. Construcc. 73 [351], e322. https://doi.org/10.3989/mc.2023.325822.

RESUMEN: *Análisis de dos montajes experimentales para estudiar la fractura en modo II con probetas entalladas de yeso reforzado con fibras.* El principal objetivo de este trabajo es estudiar dos relevantes montajes experimentales diseñados para estudiar la rotura a cortante y comprobar si permiten estudiar la evolución de la fractura en Modo II y no sólo inducir una rotura por cortante al comienzo del proceso de fractura. Se han empleado dos ensayos, un ensayo estandarizado descrito en la normativa japonesa, referido aquí como JSCE, y el ensayo de push-off. Los ensayos se han realizado sobre probetas de yeso reforzado con fibras, empleando varias proporciones de fibras de polipropileno y se han monitorizado mediante correlación digital de imágenes (DIC). Los resultados muestran que es relativamente sencillo inducir una rotura en modo II con ambos ensayos pero, una vez se inicia la fractura, es extremadamente difícil lograr una evolución del proceso de fractura en condiciones de Modo II. En general, el Modo II tiene una fuerte influencia en el comienzo de la fractura, pero posteriormente el Modo I predomina.

PALABRAS CLAVE: Modo II; Cortante; Ensayo push-off; Correlación Digital de Imágenes; Yeso reforzado con fibras.

1. INTRODUCTION

This study is focused on studying two relevant experimental setups and determine if any of them help to identify the evolution of fracture under Mode II conditions in fibre-reinforced quasibrittle materials, more specifically, fibre-reinforced gypsum. In this section, the importance of fibre reinforcement in construction materials is briefly discussed, then, in order to explain the motivation of this study, a short literature review on Mode II fracture in quasibrittle materials is presented.

1.1. Fibre reinforcement of quasibrittle materials

The use of fibres as reinforcement in construction materials is not new, but has attracted the interest of many researchers and practitioners in recent years. Concrete is probably the most developed material in this sense, given that the national and international standards (1-3) already provide guidelines for their use as structural reinforcement, which has boosted their usage in recent projects. The benefits of the addition of fibres in quasibrittle matrices are well known and, in the construction field, fibre-reinforced concrete (FRC) is used as provisional interior lining of tunnels during their construction process, as well as in precast concrete elements that are exposed to tension stresses when they are stored or transported to the work site.

In recent years new polymer fibres have started to be used as structural reinforcement of concrete, providing good strengthening properties and not suffering from important disadvantages of traditional steel fibres, such as corrosion, which can be of paramount importance in certain architectural applications, or electric transmissivity, which may limit their use in certain precast elements, such as railway sleepers. Some polymer fibres have proved to be a promising alternative to steel fibres, providing good mechanical properties to FRC under tensile stresses and in different manufacturing conditions (4-6), which has motivated their use in some initial applications as structural reinforcement (7, 8). The main mechanisms that lead to their good reinforcing performance are already identified, with the fibre length and the mechanical properties of the polymeric material being the most relevant.

Although concrete attracts most research efforts regarding fibre reinforced construction materials, gypsum can also benefit from this technology. Gypsum is the most widely used material as interior lining in buildings due to, among other reasons, its low cost, easy manipulation, its versatility with different finishes and formats and its hygroscopic and good aesthetic properties. The industry of gypsum has evolved through time, finding new applications and products, such as gypsum plasterboard, which has allowed using this material in a wider range of applications of the construction industry. Nevertheless, not big advances can be observed over the past two decades, and the use of fibres could help extend the use of this material.

There are studies about the mechanical properties of fibre-reinforced gypsum (FRG), such as those by García-Santos (9, 10), that analyse how the mechanical properties of gypsum are enhanced with different polymeric fibres. Those studies are old (more than 30 years now) and do not include information about material fracture properties. An interest in using natural fibres, such as flax and hemp, can be observed in recent works, which produces mixes with better mechanical properties and better thermal and acoustic isolation conditions, representing environmentally friendly solutions (11-13). Some other studies analyse the use of polymer fibres as gypsum reinforcement (14, 15) or the influence of graphite filler additions (16), which not only affect the mechanical properties of the mix, but also its thermal isolation properties.

In general, when FRG properties are studied, mechanical tests are usually limited to studying compressive strength, elastic modulus and flexural strength. Nevertheless, fracture energy absorbed by the material before failure can be of great importance in some fields, such as seismic and impact events or differential settlements in structures. In such situations, knowing and modifying the energy that a certain material can absorb before their eventual failure is of great importance in order to design strategies that may increase safety, reduce economic losses or even mitigate the social alarm that the appearance of cracks in building partitions may cause. In this sense, fracture energy is one of the material properties that are notably enhanced with the addition of fibres in gypsum (15).

1.2 Mode II fracture in quasibrittle materials

Fracture of quasibrittle materials has attracted the attention of many researchers over the last decades, which has allowed understanding the mechanisms involved. When dealing with fracture, three modes are identified, with Mode I corresponding to crack opening perpendicular to the crack direction and being related fundamentally to normal stresses along the crack propagation, Mode II corresponding to a crack lips displacement in parallel to the crack direction and being related mainly to shear stresses, and Mode III corresponding to a crack lips displacement out of the plane of the fractured element.

There exist many studies and references dealing with Mode I, probably because it is the most usual fracture mechanism in this type of materials. These studies have helped to design reliable experimental tests that measure the parameters that drive this phenomenon, such as the three point bending test (17). From the numerical side, many fracture models have been proposed over the last decades to reproduce fracture, such as those based on the cohesive zone model (18-21), which can reproduce fracture with remarkable simplicity and accuracy. Some of these models have been adapted in recent years to reproduce fracture of fibre-reinforced quasibrittle materials (22, 23) with numerical methods such as the finite element analysis.

Nevertheless, in some occasions fracture results from a combination of modes I and II. In this regard, mode II fracture has been studied less often and not many examples can be found in the literature, partly because mode I fracture is more usual and partly because it is harder to experimentally induce fracture under mode II conditions. From the experimental point of view, some studies have proposed tests to analyse shear fracture, such as the experiment proposed by Nooru-Mohamed (24, 25), which allows combining Mode I and Mode II conditions. Other experimental tests aiming to study shear fracture in concrete are described in (26), two specifically: a test described in the Japanese standard JSCE-G 553-1999 (27) and the push-off test, that has been lately used with success for analysing shear fracture in fibre-reinforced-concrete (28-30). From the point of view of numerically reproducing fracture, some models include the effect of the combination of Modes I and II, like (31-33). These models need parameters to define the fracture behaviour under Mode I and under Mode II. While parameters driving Mode I fracture (mainly tensile strength f_t and fracture energy G_F) can be obtained experimentally with standardised tests (17, 34), parameters related to Mode II are usually estimated, since their experimental measurement is not easy to obtain.

This work aims to deepen the knowledge of the mechanisms involved in fracture of a specimen subjected to pure shear stresses. To do this, FRG specimens are used and their performance is compared with that of plain gypsum specimens. FRG specimens are reinforced with polypropylene fibres, usually employed in concrete to prevent cracking due to shrinkage, and three fibre proportions are analysed: 5, 10 and 20 kg/m^3. To induce shear stresses, two tests are employed, one of them corresponding to a standardised test described in the Japanese norm (27), that will be here referred to as JSCE test, and the push-off test, that has been lately used to successfully analyse shear fracture in fibre-reinforced concrete (29, 30).

2. DESCRIPTION OF THE STUDY

As mentioned above, three FRG mixes have been analysed and compared with a plain gypsum mix, thus, four mixes have been prepared and their composition can be consulted in Table 1. Plain gypsum reference mix is identified as 0 and the rest of mixes are identified as A followed by 5, 10 or 20, depending on the fibre proportion used. In all cases, a water/gypsum ratio of 0.63 is used; this value was obtained following the procedure described in the UNE-EN 13279-2 standard (35) which determines the mass of gypsum that can be saturated when it is sprinkled into 100 g of water and can be summarised as follows: 100 g of water are poured in a glass vessel with an inner diameter of 66 mm inner and two marks at heights of 16 and 32 mm from the base. The procedure lasts 120±5 seconds and can be divided into four steps:

1. Gypsum is sprinkled over the water surface for around 30 seconds until the first mark is reached.
2. Gypsum is sprinkled for around 30 seconds until the second mark is reached.
3. Gypsum is sprinkled for around 30 seconds until the gypsum plaster that forms in the vessel reaches a level of 2 mm under the water surface.
4. During the remaining 20-40 seconds, gypsum is sprinkled until the water layer disappears.

Table 1. Composition of the four mixes used in this study.

Mix	w/g	Fibres proportion (kg/m^3)
0	0.63	0
A5	0.63	5
A10	0.63	10
A20	0.63	20

The specimens were manufactured following a slight variation of the procedure described in UNE-EN 13279-2 for adding the fibres. Such procedure is described below:

1. Gypsum was poured on the water and manually mixed for 40 seconds.
2. Fibres were added and mixed manually for 20 seconds.
3. Mixing continued for 60 more seconds in a planetary mixer at low speed.
4. Moulds, previously impregnated with release agent, were filled.
5. Moulds were hit to eliminate air bubbles and finally levelled.
6. The specimens were unmoulded and cured inside a controlled-climate chamber for seven days at 23±2ºC and relative humidity of 50±5\%.
7. Specimens were dried inside an oven at 50ºC for 48 hours.
8. Specimens were cooled at room temperature and the notch was cut with a band saw by dry way.
9. Specimens were marked with black spray for the later use of digital image correlation (DIC).

2.1. JSCE test

Figure 1a shows the scheme of this test. A prismatic specimen is doubly notched in two cross sections and is supported on two points in its lower side and load is applied on two points in the upper side, thus inducing shear stresses in the vertical ligaments defined by the four notches. External supports placed on the upper side of the specimen ensure absence of bending during the load application.

2.2. Push-off test

Figure1b schematically shows the configuration of this test. A Z-shaped specimen is used and a uniaxial compression is applied by means of point load in the upper side and a point support in the lower side. The vertical ligament of length *d* is then subjected to high shear stresses. This test, as the work by Picazo et al. shows (29, 30) is very sensitive to small load misalignments, thus a very precise preparation of the test is necessary. Furthermore, the upper support where load is applied must ensure that no additional torque is applied, so ball joints or similar solutions must be employed; here a double cylinder joint has been used.

3. MATERIALS AND METHODS

3.1. Materials

Gypsum used in this work is plaster, classified as A1, according to the EN 13279-1 standard (36). It is a fine-grained high quality gypsum with a purity over 90%, composed by hemihydrate calcium sulphate ($CaSO_4 \cdot 0.5\,H_2O$) and is commonly used for manufacturing precast elements, such as plasterboard panels used in sandwich-type partitions.

The fibres used here are polypropylene microfibres, named Sikafiber M-12, that are usually employed in concrete and mortars for reducing their cracking and increasing their durability. They are 12 mm long and their diameter is 31 µm; the aspect of these fibres can be observed in Figure 2.

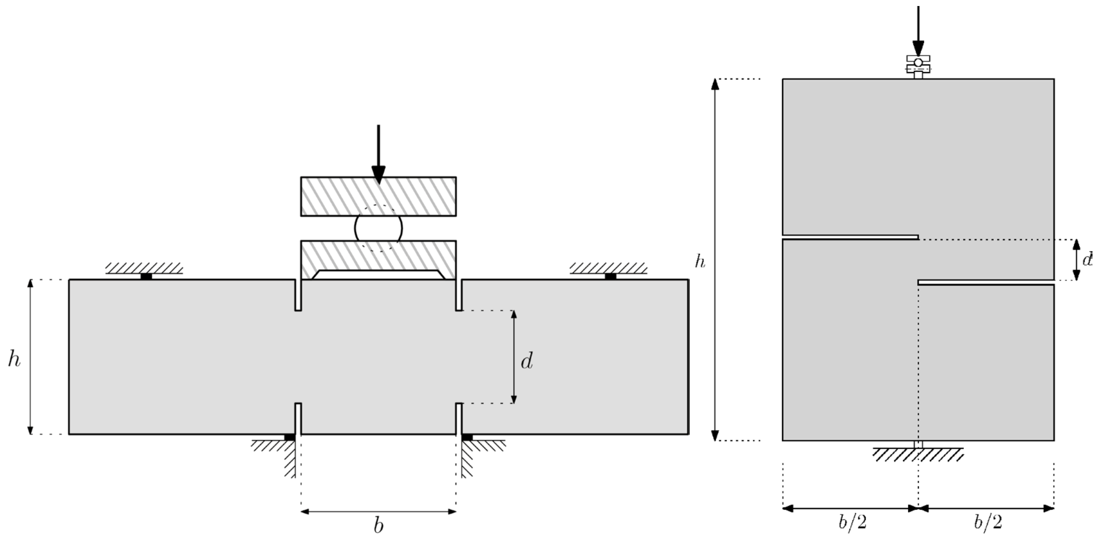

(a) JSCE test (b) Push-off test

Figure 1. Schemes of the tests used in this work.

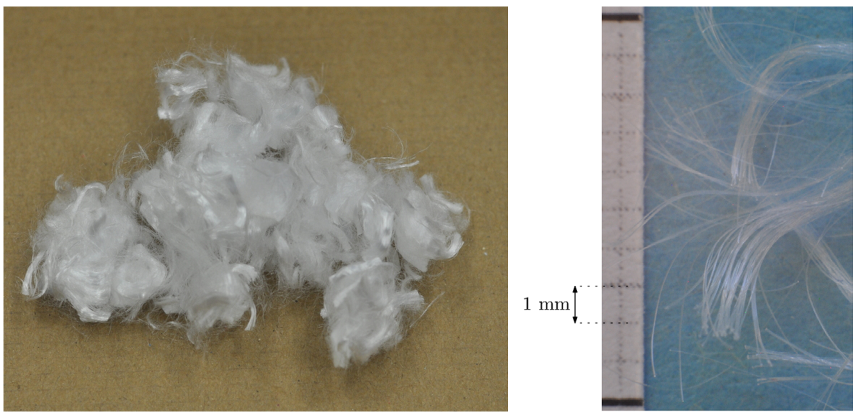

Figure 2. Polypropylene fibres used as reinforcement in the FRG specimens.

These materials were combined with water to produce the mixes described in Table 1. To produce the plain gypsum mix, the procedure described in the EN 13279-2 standard (35) was used and, to produce FRG mixes, a slight variation of it already employed in previous works (15, 37), which includes the addition of fibres in the last 20 seconds of the manual mixing.

3.2. Experimental setups and methodology

In this section the experimental setups employed in both types of tests are described. All tests were carried out with a dual column testing system of Instron of the 5960 series and using a load cell of 30 kN of capacity. All tests were analysed with digital image correlation (DIC) which provides interesting information in this type of materials when fracture is analysed (15, 38). In this case a Mako U-130B video camera with a resolution of 1280 x 1024 pixels and the software Vic-2D, by Correlated Solutions (39) have been used. Digital image correlation in 2D was performed by employing a 21 pixels size facet and 5 pixels of step.

3.2.1. JSCE test

Prismatic specimens of 160 mm x 40 mm x 40 mm were manufactured and four notches produced by means of a band saw. The resulting geometry, according to parameters shown in Figure 1a corresponds to h=40 mm, b=40 mm and d=24 mm. Twelve specimens were tested, three per mix (0, A5, A10 and A20). Specific steel fixtures were manufactured for this test so that the supports disposition shown in Figure 1 could be reproduced. Figure 3 shows the final experimental setup. To ensure applying a centred load and avoid possible unwanted torques induced by a lack of parallelism between the support lines at the bottoms and those at the upper side, load was transmitted through a ball joint.

Load was applied with a displacement control of 0.25 mm/min up to a maximum displacement of 3 mm and images for DIC were captured every 5 seconds.

3.2.2. Push-off test

For this test, 40 mm thick specimens were manufactured and two notches produced with a band saw, resulting in specimens with the shape shown in Figure 1b. Notches were extremely carefully produced in order to ensure good alignment with load and avoid unwanted torsion effects. For this test, two types of specimens were manufactured, which will be described later; their dimensions, according to parameters of Figure 1b are shown in Table 2. The reason that motivated manufacturing of different types of specimens include strategies for improving the experimental results that will be explained further in Section 4.2.

Table 2. Dimensions of push-off specimens according to parameters on Figure 1b.

	h (mm)	b (mm)	d (mm)
Type 0	160	128	10
Type 1	85	64	14

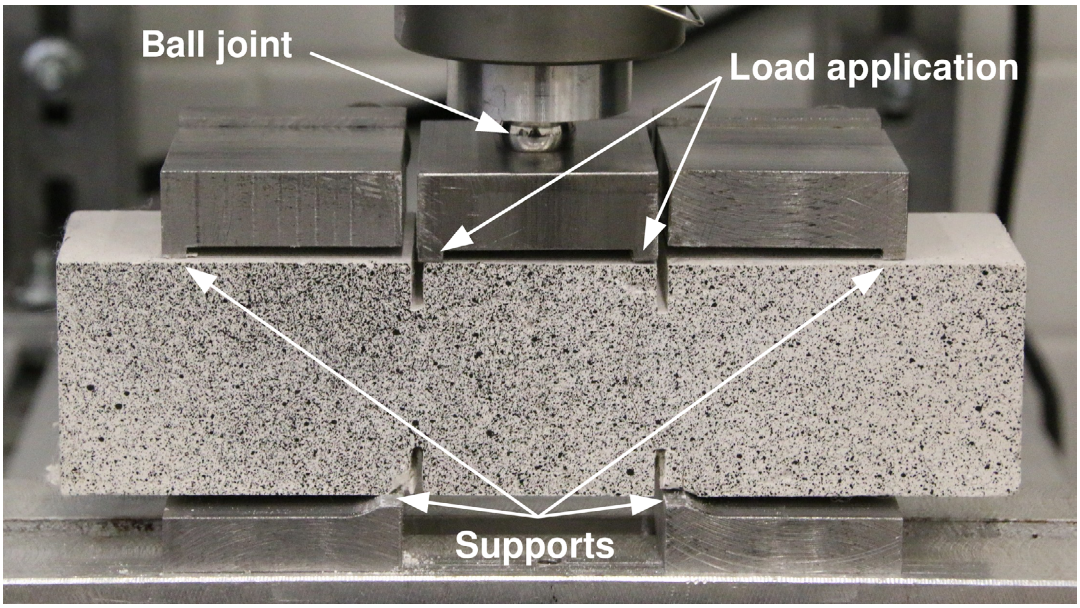

Figure 3. Setup of the JSCE test.

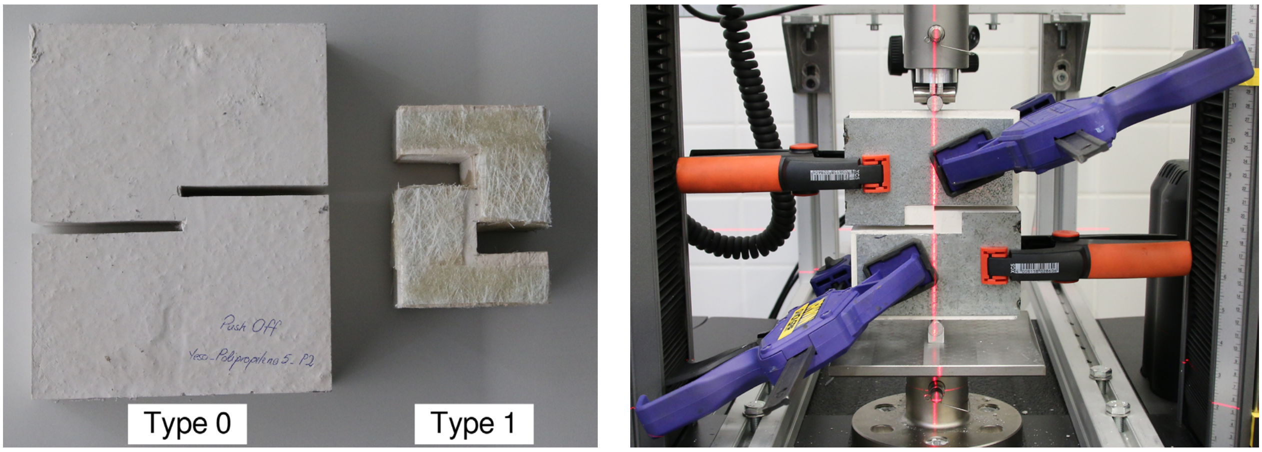

Figure 4. (a) Type 0 and Type 1 specimens of the push-off test; (b) Experimental setup of the push-off test.

This test was carried out with two different geometries and specimens were prepared differently in each case. Each geometry will be referred to as Type 0 and Type 1 hereafter. Figure 4a shows each of these geometries and Table 2 their dimensions according to parameters defined in Figure 1. A first set of twelve specimens were manufactured with Type 0 geometry, three per mix (0, A5, A10 and A20), and a second set of six specimens manufactured with Type 1 geometry, two for each of mixes A5, A10 and A20.

As Picazo et al. report in (29), this test tends to generate flexural stresses at the internal sides of the notches, to avoid this, some regions of the specimen must be reinforced. Figure 5 shows the S11 and S12 stress fields, which corresponds to σ_x and τ_{xy} components of the stress tensor, respectively, obtained with a finite element model that reproduces the push-off test for an elastic specimen of the same geometry as Type 0 specimens shown in Figure 4. There is a high concentration of shear stresses along the vertical ligament where shear fracture is expected, but high tensile stresses can be observed in the horizontal notches due to flexural strains in the upper and lower cantilevers of the specimen.

Type 0 specimens are larger, have thin notches of around 4 mm and were tested using an external steel reinforcement fixed by means of hand clamps, as can be observed in Figure 4b. This disposition had some benefits, like easier preparation and a larger visible area in the region of interest defined by both notches, where Mode II fracture is expected. Nevertheless, it also had some disadvantages, as will be discussed later.

Type 1 specimens are smaller, have thicker notches of around 15 mm and were reinforced with external glass fibre reinforcement fixed with polyester resin. The purpose of this external reinforcement is avoiding unwanted Mode I fracture due to flexural stresses (see Figure 5). Thicker notches allowed reinforcing internal sides of notches and some additional benefits, although they also presented some disadvantages, as it will be observed later.

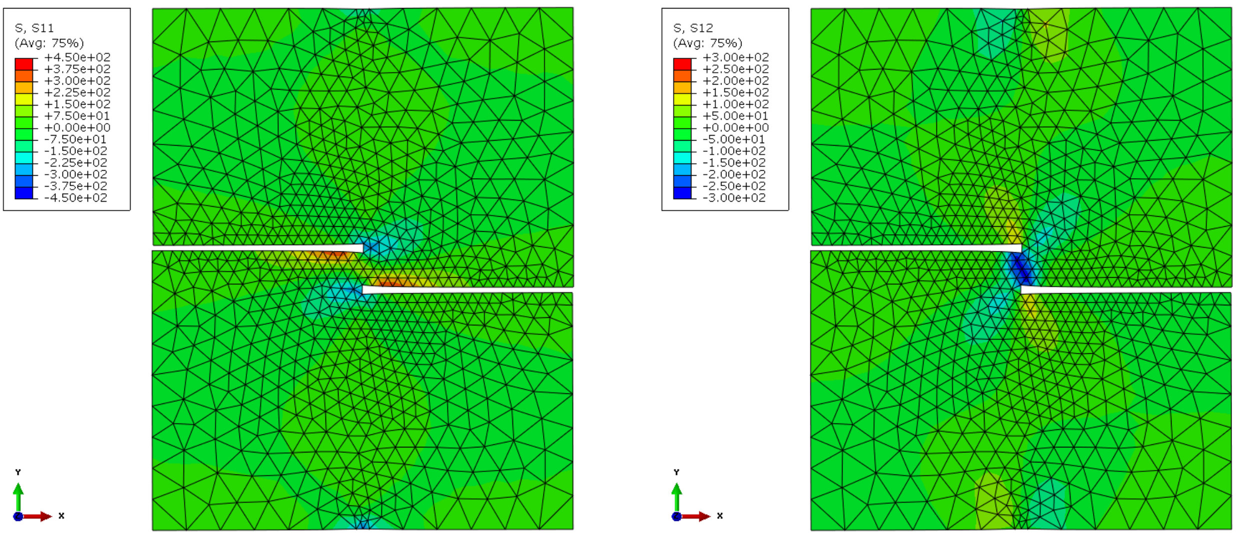

Figure 5. S11 (σ_x) and S12 (τ_{xy}) fields obtained with an elastic finite element model of the push-off test.

4. RESULTS

In this section, the experimental results are presented. Firstly, the results obtained with the JSCE test will be shown and later the results corresponding to both specimen types of the push-off tests will be presented.

4.1. JSCE test

Figure 6 shows the load-displacement diagrams of all the tested specimens. Plain gypsum specimens are represented in grey and A5, A10 and A20 FRG mixes are represented in blue, green and red, respectively. Line formats allow identification of different specimens of the same mix.

Fibre reinforcement results in higher strength and, although some general trends can be identified, no clear differences between increasing fibre proportions can be observed, especially between mixes A5 and A10. In all FRG mixes, the peak load is higher when compared with plain gypsum specimens; nevertheless, interpreting these results is not trivial. In all FRG specimens several load drops and load increments are observed along the test, although these are more evident in A5 and A10 specimens, since A20 specimens present an almost constant load increment after an initial elastic behaviour. Finally, it is interesting to note that material ductility is greatly enhanced by fibre addition, ductility increases with fibre proportion, but is also relevant even with small proportions of fibres.

If A5 specimen represented with a solid line in Figure 6 is observed, all the main failure mechanisms that take place during the test can be identified:

- Load initially increases linearly with the displacement, which corresponds to an elastic behaviour before any damage develops in the specimen.
- Just after the linear behaviour ends, an almost horizontal plateau is observed, which is related to local damage around some supports.
- The first load drop (between points 1 and 2) identifies the first crack at one of the notches. Once it is produced, load increases again due to the fibre reinforcement (between points 2 and 3), which strengthens the cracked region.
- The second load drop (between points 3 and 4) identifies the appearance of a second crack, after which, again, fibre reinforcement allows a new load increment.

Figure 7 shows the ε_x and ε_{xy} strain fields obtained with the digital image correlation technique for this specimen (first specimen of A5 mix) at four representative instants of the load-displacement diagram, that are identified by numbers 1 to 4 in Figure 6:

- Point 1: This point identifies the instant just before the first load drop is observed. The DIC images show that, apart from local damage around the supports and the load application points, shear strain (ε_{xy}) concentrates along both vertical planes defined by notches. Note that the extreme values of the colour scale identify the same shear strain, although of different sign, which implies that both vertical planes are subjected to similar shear strains. Regarding the shear strain fields (right images in the figure), shear strain seems to be quite uniform along the shear plane defined by the notches on the left, but not in the plane defined by the notches on the right, where the onset of fracture modifies the distribution of stresses. On another note, ε_x strains suggest that the portion of the specimen between both vertical shear planes is subjected to bending, since the ε_x strain field presents compression strains at the upper half and tension strains at the lower half.
- Point 2: These results correspond to the first frame after the first load drop. The DIC images show clearly the initiation of the first crack, which occurs at the

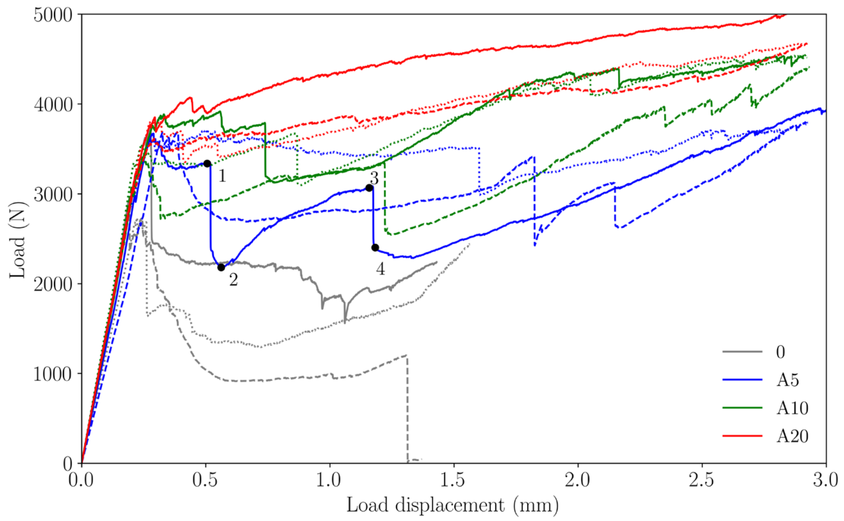

Figure 6. Load-displacement diagrams obtained with the JSCE test. Mixes are identified with different colours.

bottom notch of the right plane. The ε_x strain field shows a very high concentration of these strains along the crack, which, since the crack is mainly vertical, evidences a crack opening where Mode I plays an important role together with Mode II.

- Point 3: Just before the second load drop, the DIC images show that the first crack has evolved under a combination of Mode I and Mode II, with the former being the predominant mode. In the left vertical shear plane, there is again a high concentration of shear strains.
- Point 4: These results show the strain fields just after the second load drop. A new crack appears at the left vertical shear plane, which is responsible for this second load drop.

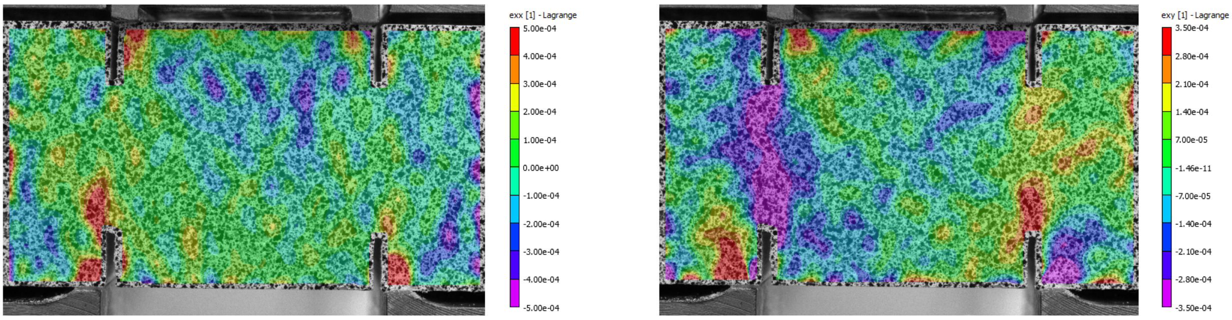

(a) Point 1 in Figure 6: (left): ε_x, (right): ε_{xy}.

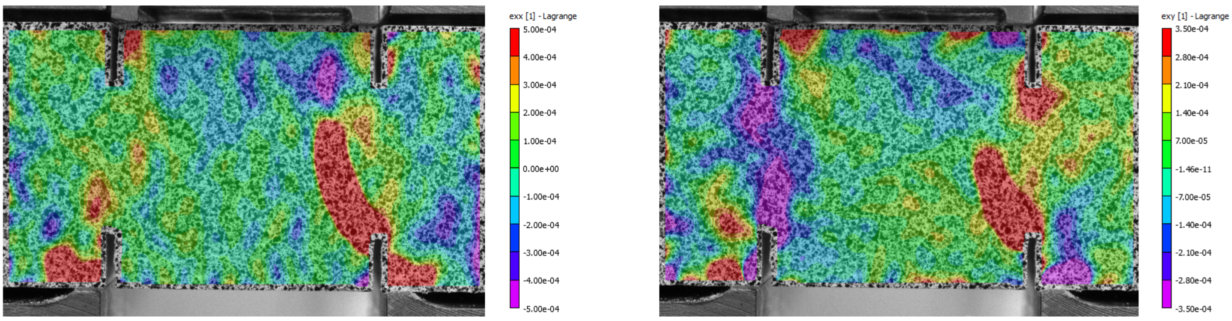

(b) Point 2 in Figure 6: (left): ε_x, (right): ε_{xy}.

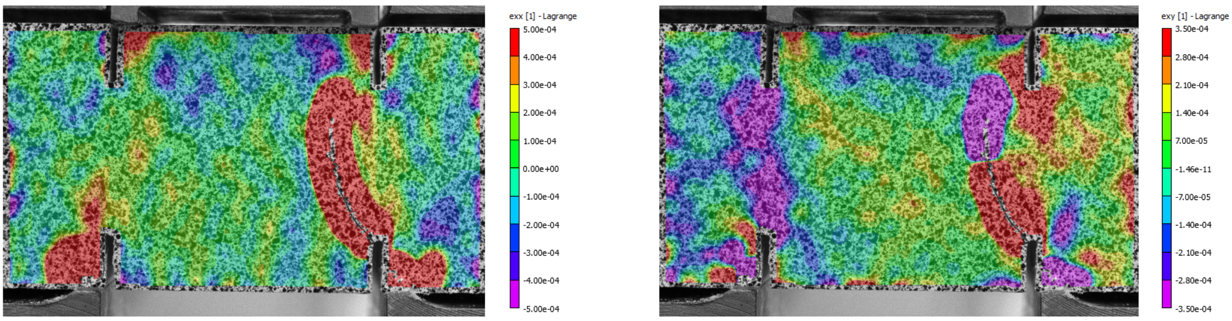

(c) Point 3 in Figure 6: (left): ε_x, (right): ε_{xy}.

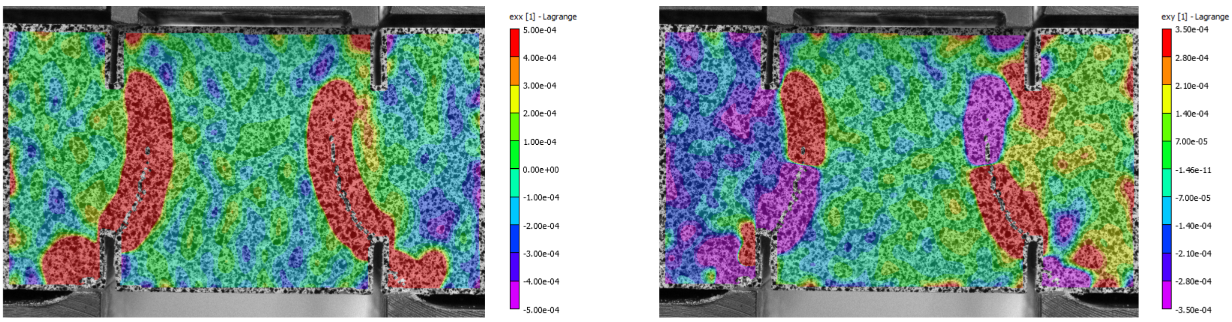

(d) Point 4 in Figure 6: (left): ε_x, (right): ε_{xy}.

FIGURE 7. Strains field ε_x (left) and ε_{xy} (right) of specimen 1 of A5 mix at four instants during the JSCE test, identified by points 1 to 4 shown in Figure 6.

In this test, several issues make interpretation of the experimental results difficult. First of all, each specimen has two possible fracture planes, which makes it hard to measure material fracture properties. Secondly, in the case of FRG, local damage develops around the supports, which affects the resulting load-displacement diagram. Thirdly, fracture develops in several places along the test, up to four possible cracks. Finally, if the displacement is large enough, the central region of the specimen usually rotates, which modifies the way load is transmitted in the specimen; for example, when this rotation is large enough, the central portion of the specimen contacts the lateral portions, therefore, the load is not only transmitted along the vertical planes defined by the notches, but also through these contacts, thus resulting in a complex load transmission that no longer permits the study of Mode II fracture.

In addition to the previous issues, the way cracking develops in each of the cracks produced during the test suggest that fracture is due to a combination of Modes I and II, since crack lips do not move in parallel to each other, but an evident crack opening in perpendicular to them is clearly observed. Therefore, even if all the issues mentioned above could be avoided, the resulting fracture process would not serve to measure Mode II fracture, since Mode I would also be involved.

4.2. Push-off test

Figure 8 shows the shear stress-displacement diagrams obtained with the Type 0 specimens. Assuming a uniform distribution of shear stresses, the value of the shear stress τ is obtained as load divided by the area of the ligament subjected to shear:

$$\tau = \frac{P}{d \cdot t} \qquad [1]$$

where *P* refers to the load, *d* represents the ligament length (see Figure 1) and *t* the specimen thickness, which in this case equals 40 mm.

As in Figure 8, each colour identifies each mix, with the grey colour identifying the plain gypsum specimens and blue, green and red identifying A5, A10 and A20 mixes. Three specimens of each mix have been tested, each specimen of a mix has a different line format to allow easy identification.

These results show an important experimental scatter, usual in this type of material. The most remarkable effect of fibre reinforcement can be observed in how the load drop after the peak load becomes smaller as the fibre proportion increases.

Apart from the load-displacement diagrams, when the digital image correlation results are analysed, if the horizontal direction is identified as the *x* axis and the vertical direction as the *y* axis, before fracture takes place, shear strain ε_{xy} is high along the vertical ligament where Mode II fracture is expected but, once fracture occurs, two unwanted issues are identified:

- Fracture often occurs outside the vertical ligament where shear fracture is expected.
- Crack develops with crack lips moving apart from each other, not in parallel, thus revealing a Mode I fracture, rather than a fracture evolution in Mode II.

Figure 9a) shows the ε_x and ε_{xy} strain fields just before the onset of fracture, revealing that shear strain is high along the vertical shear ligament, although horizontal strains appear along the horizontal notches. Therefore, three fracture mechanisms are in competition: the shear failure along the vertical ligament and the tensile failure on both horizontal notches.

Finally, as shown in 9b), failure develops in one of the horizontal notches, which means that failure

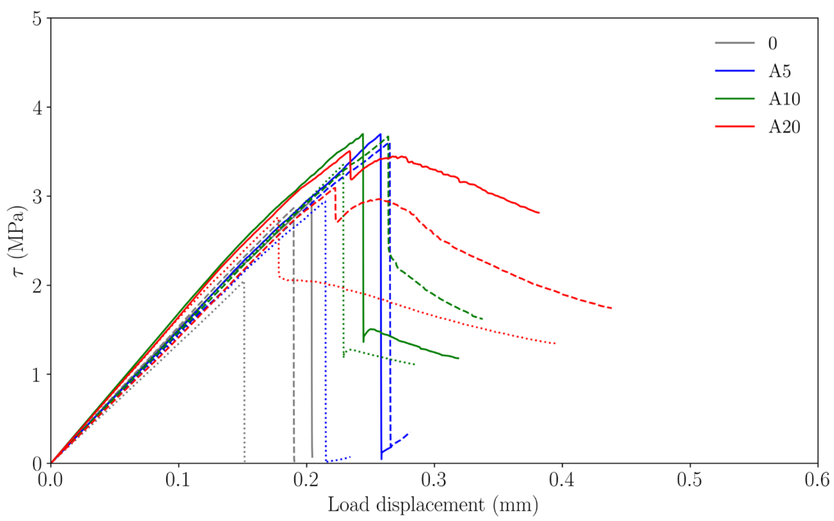

Figure 8. Load-displacement diagrams obtained with the push-off test using Type 0 specimens (see Figure 4a). Mixes are identified with different colours.

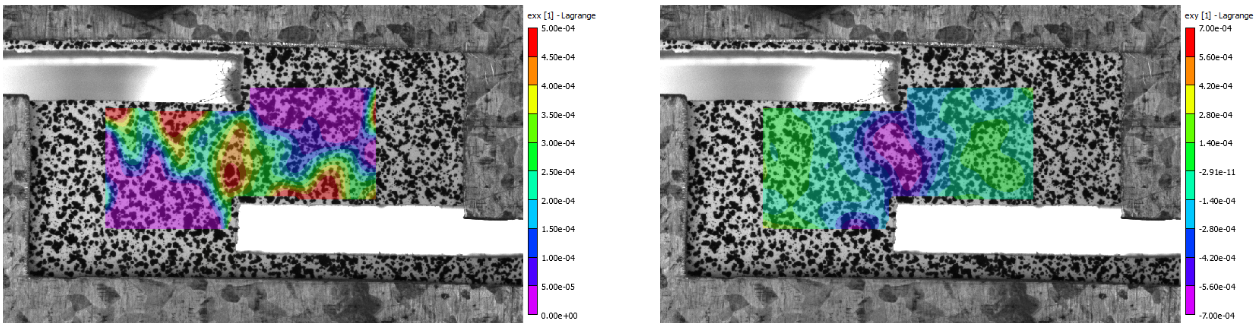

(a) Strains field of one specimen of A5 mix just before fracture occurs; (left): ε_x, (right): ε_{xy}.

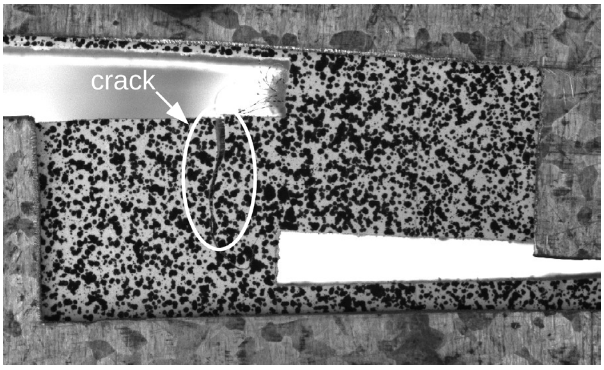

(b) Image of the specimen once fracture has developed.

Figure 9. (a) Strains fields of one specimen of A5 mix just before fracture occurs and (b) image of the specimen once fracture has developed. The circle shows that crack has not developed along the shear plane.

does not occur due to shearing but due to indirect tensile stresses induced by bending of the cantilevers. As Figure 9b) also shows, the crack develops mainly under Mode I conditions, since the crack lips fundamentally move apart from each other in perpendicular to the crack path.

These results suggest that, although the specimen is subjected to shear loading and, in fact, a high concentration of shear stresses is reached along the vertical ligament before the onset of fracture, fracture eventually takes place in another region and develops as Mode I fracture. Therefore, these results are not providing information about Mode II fracture development. On another note, as fracture develops, both halves of the specimen rotate around the crack until two lips of a notch contact each other, then providing no longer valid results of the test.

These issues are the reason why a new set of specimens are tested using the Type 1 geometry shown in Figure 4a. This geometry allows reinforcing the sides of the notches where flexural stresses lead to unwanted Mode I fracture and permits carrying out the test up to larger load displacement values, providing more complete test results.

Figure 10 shows the shear stress-displacement diagrams obtained with the Type 1 specimens, which were carried out only with FRG mixes. These diagrams show a remarkably different behaviour between mixes, with a general trend showing that increasing proportions of fibres leads to higher ductilities, as observed in the case of the JSCE test, but some results are, in principle, unexpected. In all mixes, very different behaviours can be observed between each pair of specimens and, apparently, specimens of different mixes have a very similar behaviour between each other, but very different with respect to the other specimen of the same mix. For example, results marked with I in the figure correspond to different mixes but have a quite similar post-peak behaviour, which is the part of the diagram more influenced by the fibre addition. Likewise, results marked with II also correspond to different mixes and also have a very similar behaviour if compared with each other, being different to the other specimens of the same mixes. This can be explained by observing the images obtained during the tests. Figure 11 shows two images that help to understand these differences and why some results cannot be considered as valid:

- Results identified with I in Figure 10 correspond to the case shown in Figure 11a, where fracture does not develop along the vertical shear plane, but inside the reinforced region, that is why fracture cannot be observed in this image, since it is hidden by the glass fibre reinforcement.
- Results identified with II in Figure 10 fails as shown in Figure 11b. These specimens do fail along the vertical shear plane, as expected, but crack does not develop under mode II condi-

tions. Once crack opens, fracture develops under Mode I conditions, since the upper half and the lower half of the specimen rotate around each other, thus crack lips separate from each other perpendicularly to the crack path.

Regarding the result identified with III in Figure 10, the test is clearly invalid since fracture does not take place along the vertical shear ligament, but in the lower cantilever where the lower support is applied.

Finally, the result identified with IV in Figure 10 corresponds to a specimen in which fracture does take place along the vertical shear ligament and develops as shown in Figure 12. These results show the evolution of three fields: ε_x and ε_{xy} strain fields and the vertical displacement field *v* in this specimen at different stages of the test, where a) is the instant just before the load drop occurs and results b) and c) are two subsequent instants. Fracture evolves with high concentration of shear strain ε_{xy} along the vertical ligament and, differently from other cases like the one shown in Figure 9b), where fracture developed in clear Mode I conditions, here Mode II is predominant, which can be observed in the evolution of the vertical displacement field *v*. Just before fracture, no relative vertical displacement can be observed between the left and right halves of the specimen, but once fracture starts, both halves clearly move vertically with respect to each other along the vertical ligament (note the evolution of the *v* field in Figure 12). Finally, if the evolution of ε_x is observed, Mode I is also present, although its relevance is less important than in other cases.

These results suggest that in this specimen, not only the onset of fracture is strongly influenced by shear stresses, which also happened in other specimens (see Figure 9), but fracture also evolves strongly due to shearing, following a similar evolution as expected for Mode II (see Figure 1). Nevertheless, this shearing is not pure, and tensile stresses, associated with Mode I, is also present, although with a smaller relevance than in other specimens where fracture mainly occurred under Mode I conditions (see Figures 9b and 11b).

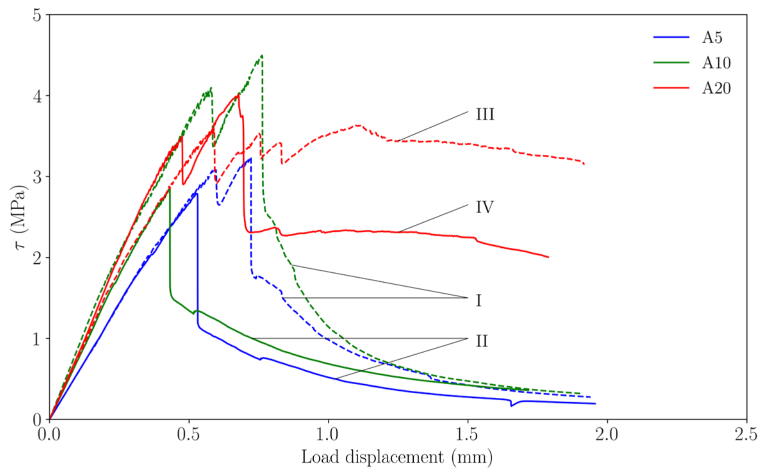

Figure 10. Load-displacement diagrams obtained with the push-off test using Type 1 specimens (see Figure 4a). Mixes are identified with different colours.

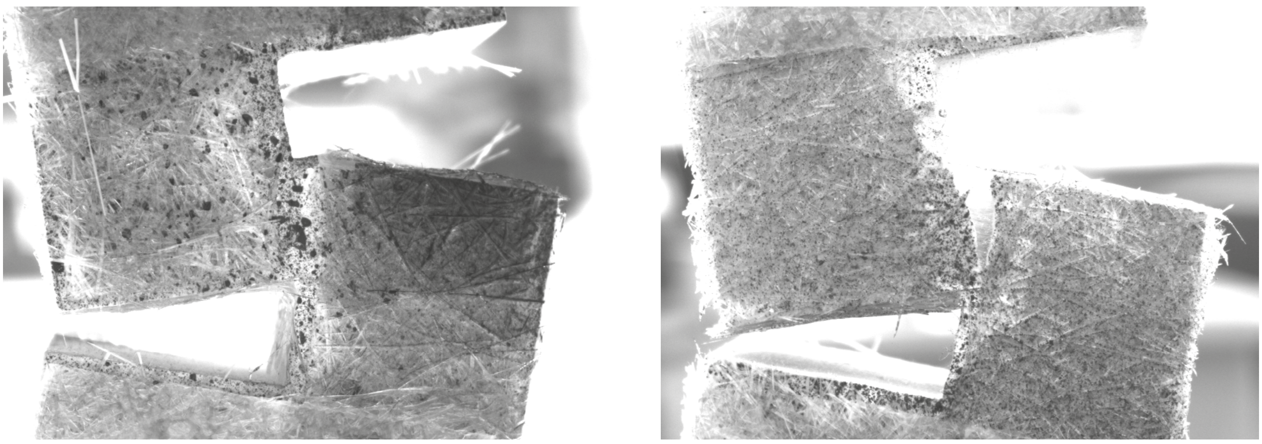

(a) One of the specimens marked with I in Figure 10.

(b) One of the specimens marked with II in Figure 10.

Figure 11. Last frames of two push-off tests on Type 1 specimens.

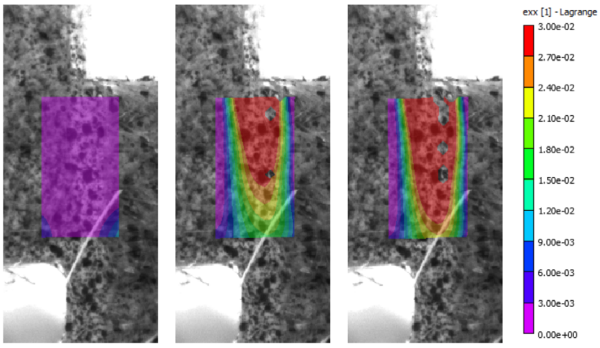

(a) ε_x: (left): instant before load drop occurs, (center) and (right): subsequent instants.

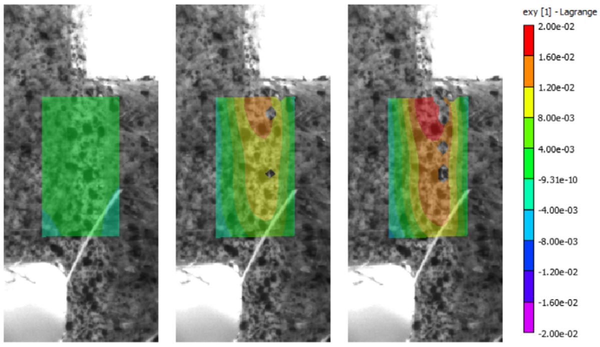

(b) ε_{xy}: (left): instant before load drop occurs, (center) and (right): subsequent instants.

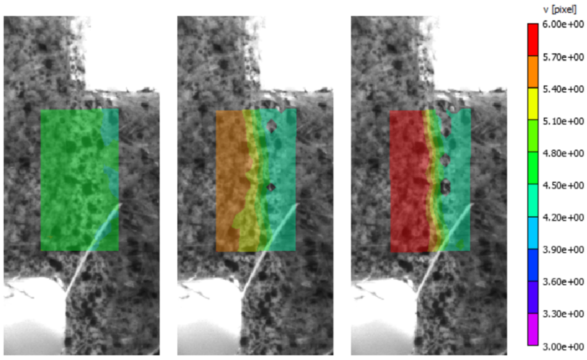

(c) v: (left): instant before load drop occurs, (center) and (right): subsequent instants.

Figure 12. Evolution of the ε_x and ε_{xy} strain fields and the vertical displacement field v for the specimen of the A20 mix identified with IV in Figure 10.

4.3 Comparison between both tests

In the previous sections both tests have been analysed independently, providing understanding on how to interpret the experimental results. The aim of this section is to compare the results obtained with both tests to see if they provide similar values. To do this, the shear stress-displacement diagrams are compared. The shear stress is obtained as load over shearing surface, which in the case of the push-off test is provided by Equation [1], while in the case of the JSCE test, with two shearing surfaces, is obtained with Equation [2].

$$\tau = P/(2 \cdot d \cdot t) \qquad [2]$$

Figure 13 compares the shear stress-displacement diagrams obtained with both tests. Results are presented for each fibre proportion and with the same colour code used in previous figures; diagrams obtained with the JSCE test are depicted with dashed lines while results obtained with the push-off test are depicted with solid lines.

As commented before, the JSCE test is hard to analyse after the peak load, so the main comparison can be made on the load that induces fracture for the first time. If this value is compared, a big difference can be observed between both tests for all three fibre proportions. In all cases, the peak load is higher if the push-off tests is used, which is probably related to the main difference between both experimental setups, that induce shear stresses in different number of planes. Since the push-off test induces shear in only one plane, the peak load of the test can be directly related to the shear capacity of the material. On the contrary, the JSCE test induces shear in two planes at the same time and the peak load identifies fracture initiation in one of them, therefore such load cannot identify the maximum shear capacity of the material because part of the load is resisted by the still undamaged shear plane. The JSCE test would probably provide similar values to the push-off test if failure initiated at the same time in both shear planes, which has not happened in any of the tests carried out in this work.

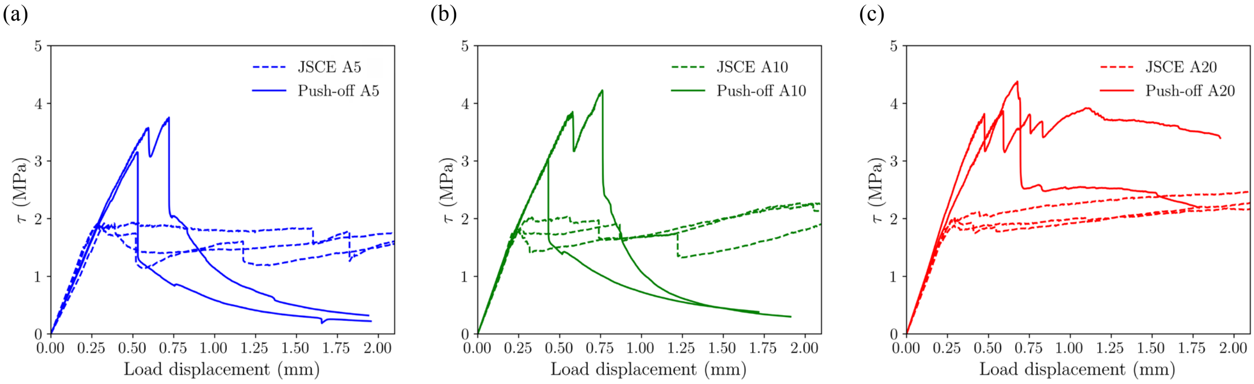

FIGURE 13. Comparison of the shear stress-displacement diagrams obtained with both tests on FRG specimens with increasing fibre proportions: (a) 5 kg/m^3, (b) 10 kg/m^3, (c) 20 kg/m^3.

5. CONCLUSIONS

5.1. JSCE test

The results obtained with the JSCE test show that an increasing proportion of fibres modify the behaviour of the material, resulting in a slightly higher initial peak load, a higher bearing capacity after it and an overall increase of ductility. Fibres act as a bonding bridge between both crack lips, thus increasing the bearing capacity of the specimen.

This test requires a quite complex experimental setup and produces results that are not easy to interpret due to the reasons mentioned in Section 4.1, like the damage around the supports or the shear damage induced in two planes at the same time. Nevertheless, it effectively induces a strong shear stress state along both vertical ligaments where fracture is expected, as DIC analysis reveals, but once fracture starts, it does not clearly evolve under pure Mode II. In fact, DIC analysis suggests that Mode I is predominant in the crack opening process. Moreover, the crack pattern resembles the results obtained with other tests like those suggested by Nooru-Mohamed (24, 25) and Bocca (40), leading to a crack opening evolution that combines Mode I and Mode II, with the former being predominant over the latter, as already observed in (41).

5.2. Push-off test

The results obtained with the push-off test also show a strengthening effect of the addition of fibres, especially after the peak load, with an interesting ductility of the material that increases with the fibre proportion.

In this test, results interpretation is not difficult, since only one fracture shear ligament is loaded and no damage previous to the peak load is observed. DIC analysis reveals that shear strain is effectively induced along the vertical ligament, but shear fracture mechanism competes with secondary bending phenomena that may lead to fracture in a different region of the specimen and lead to a different fracture process, more related to Mode I rather than Mode II.

The specimen geometry and the experimental setup must be carefully designed, since this test is particularly sensitive to any misalignment of loading, as proves the fact that only one of the specimens has produced a quite satisfactory result.

Push-off test results show that producing fracture under strong shearing conditions is relatively easy with this experimental setup, but fracture evolution under Mode II conditions is extremely hard to obtain. Only one of the more heavily reinforced specimens (A20 mix) has resulted in a fracture evolution quite similar to the theoretical Mode II, but even in this case, Mode I has also a relevant role, as DIC results prove (see Figure 12).

5.3. Comparison of results

As a final conclusion, although both tests induce shear fracture in the specimens, their results cannot be directly compared, as shown in Section 4.3. The push-off test induces fracture in an only shear plane and the results can be directly related to the fracture evolution of that plane. Nevertheless, the JSCE test induces shear stresses in two planes at the same time, which fail at different displacement values during the test, which do not make possible to obtain the fracture load of an only plane and, as a consequence, obtain the shear stress value at which fracture initiates.

ACKNOWLEDGEMENTS

Authors gratefully acknowledge the financial support provided by Universidad de Jaén through Action 1 of the Support to transfer of knowledge, entrepreneurship and employability plan of this university, which has allowed carrying out the experimental tests described in this study.

AUTHOR CONTRIBUTIONS:

Conceptualization: F. Suárez. Data curation: F. Suárez, J.F. Aceituno, J. Donaire-Ávila. Formal analysis: F. Suárez, J.F. Aceituno, J. Donaire-Ávila. Funding acquisition: F. Suárez. Investigation: F. Suárez, J.F. Aceituno, J. Donaire-Ávila. Methodology: F. Suárez. Visualization: F. Suárez, J.F. Aceituno, J. Donaire-Ávila. Writing, original draft: F. Suárez. Writing, review & editing: J.F. Aceituno, J. Donaire-Ávila.

REFERENCES

1. CNR-DT 204 (2006) Guide for the design and construction of fiber-reinforced concrete structures. Consiglio Nazionale delle Riserche: Roma, Italy, 2006.
2. EHE-08, Instrucción de hormigón estructural (2008) Ministerio de Fomento, Madrid, España.
3. Fib model code for concrete structures 2010. (2013) Ernst & Sohn. Wiley: Berlin, Germany.
4. Alberti, M.; Enfedaque, A.; Gálvez, J. (2015) Comparison between polyolefin fibre reinforced vibrated conventional concrete and self-compacting concrete. *Constr. Build. Mat.* 85 182–194. https://doi.org/10.1016/j.conbuildmat.2015.03.007.
5. Alberti, M.; Enfedaque, A.; Gálvez, J. (2017) Fibre reinforced concrete with a combination of polyolefin and steel-hooked fibres. *Compos. Struct.* 171, 317–325. https://doi.org/10.1016/j.compstruct.2017.03.033.
6. Alberti, M.; Enfedaque, A.; Gálvez, J. (2016) Fracture mechanics of polyolefin fibre reinforced concrete: Study of the influence of the concrete properties, casting procedures, the fibre length and specimen size. *Eng. Fract. Mech.* 154, 225–244. https://doi.org/10.1016/j.engfracmech.2015.12.032.
7. Alberti, M.G.; Gálvez, J.C.; Enfedaque, A.; Carmona, A.; Valverde, C.; Pardo, G. (2018) Use of steel and polyolefin fibres in the La Canda tunnels: Applying mives for assessing sustainability evaluation. *Sustainability-Basel.* 10 [12], 4765. https://doi.org/10.3390/su10124765.
8. Alberti, M.G.; Enfedaque, A.; Gálvez, J.C.; Pinillos, L. (2017) Structural cast-in-place application of polyolefin fiber–reinforced concrete in a water pipeline supporting elements. *J. Pipeline Syst. Eng. Pract*. 8 [4], 05017002. https://doi.org/10.1061/(ASCE)PS.1949-1204.0000274.
9. A. García Santos (1988) Comportamiento mecánico de yeso reforzado con polímeros sintéticos, Ph.D. thesis, Arquitectura.
10. Santos, A.G. (2009) Escayola reforzada con fibras de polipropileno y aligerada con perlas de poliestireno expandidoescayola reforzada con fibras de polipropileno y aligerada con perlas de poliestireno expandido. *Mater. Construcc.* 59 [293], 105–124. https://doi.org/10.3989/mc.2009.41107.
11. Dalmay, P.; Smith, A.; Chotard, T.; Sahay-Turner, P.; Gloaguen, V.; Krausz, P. (2010) Properties of cellulosic fibre reinforced plaster: influence of hemp or flax fibres on the properties of set gypsum. *J. Mater. Sci.* 45 [3], 793–803. https://doi.org/10.1007/s10853-009-4002-x.
12. Iucolano, F.; Liguori, B.; Aprea, P.; Caputo, D. (2018) Thermo-mechanical behaviour of hemp fibers-reinforced gypsum plasters. *Constr. Build. Mat.* 185, 256–263. https://doi.org/10.1016/j.conbuildmat.2018.07.036
13. Iucolano, F.; Boccarusso, L.; Langella, A. (2019) Hemp as eco-friendly substitute of glass fibres for gypsum reinforcement: Impact and flexural behaviour. *Compos. Part B-Eng.* 175, 107073. https://doi.org/10.1016/j.compositesb.2019.107073.
14. Zhu, C.; Zhang, J.; Peng, J.; Cao, W.; Liu, J. (2018) Physical and mechanical properties of gypsum-based composites reinforced with PVA and PP fibers. *Constr. Build. Mat.* 163, 695–705. https://doi.org/10.1016/j.conbuildmat.2017.12.168.
15. Suárez, F.; Felipe-Sesé, L.; Díaz, F.; Gálvez, J.; Alberti, M. (2020) On the fracture behaviour of fibre-reinforced gypsum using micro and macro polymer fibres. *Constr. Build. Mat.* 244, 118347. https://doi.org/10.1016/j.conbuildmat.2020.118347
16. Barbero-Barrera, M.M.; Flores-Medina, N.; Pérez-Villar, V. (2017) Assessment of thermal performance of gypsum-based composites with revalorized graphite filler. *Constr. Build. Mat.* 142, 83–91. https://doi.org/10.1016/j.conbuildmat.2017.03.060.
17. (1985) Determination of the fracture energy of mortar and concrete by means of three-point bend tests on notched beams. *Mater. Struct.* 18, 287–290. https://doi.org/10.1007/BF02472918.
18. Simo, J.C.; Oliver, J.; Armero, F. (1993) An analysis of strong discontinuities induced by strain-softening in rate-independent inelastic solids. *Comput. Mech.* 12 [5], 277–296. https://doi.org/10.1007/BF00372173.
19. Li, Y.N.; Bažant, Z.P. (1997) Cohesive crack model with rate-dependent opening and viscoelasticity: II. numerical algorithm, behavior and size effect. *Int. J. Fracture.* 86 [3], 267–288. https://doi.org/10.1023/A:1007497104557.
20. Sancho, J.M. ; Planas, J.; Cendón, D.A. ; Reyes, E.; Gálvez, J. (2007) An embedded crack model for finite element analysis of concrete fracture. *Eng. Fract. Mech.* 74 [1-2], 75–86. https://doi.org/10.1016/j.engfracmech.2006.01.015.
21. Jirásek, M. (2011) Damage and smeared crack models, in: Numerical modeling of concrete cracking, Springer, pp. 1–49. https://doi.org/10.1007/978-3-7091-0897-0_1.
22. Alberti, M.; Enfedaque, A.; Gálvez, J.; Reyes, E. (2017) Numerical modelling of the fracture of polyolefin fibre reinforced concrete by using a cohesive fracture approach. *Compos. Part B-Engineer.* 111, 200–210. https://doi.org/10.1016/j.compositesb.2016.11.052.
23. Havlásek, P.; Kabele, P. (2017) A detailed description of the computer implementation of SHCC material model in OOFEM, CTU in Prague.
24. Nooru-Mohamed, M.B. (1992) Mixed-mode fracture of concrete: An experimental approach., Ph.D. thesis, Delft University of Technology. Retrieved from http://resolver.tudelft.nl/uuid:a6a773f1-dacd-4598-aa6a-960dddf71117.
25. Nooru-Mohamed, M.; Schlangen, E.; van Mier, J.G.(1993) Experimental and numerical study on the behavior of concrete subjected to biaxial tension and shear. *Adv. Cem. Based Mater.* 1 [1], 22–37. https://doi.org/10.1016/1065-7355(93)90005-9.
26. Soetens, T.; Matthys, S. (2017) Shear-stress transfer across a crack in steel fibre-reinforced concrete. *Cem. Concr. Comp.* 82, 1–13. https://doi.org/10.1016/j.cemconcomp.2017.05.010.
27. JSCE-G 553-1999 (2005) Test method for shear strength of steel fiber reinforced concrete. Standard specifications for concrete structures. Test methods and specifications. Japan Society of Civil Engineers (JSCE), Tokyo.
28. Navas, F.O.; Navarro-Gregori, J.; Herdocia, G.L.; Serna, P.; Cuenca, E. (2018) An experimental study on the shear behaviour of reinforced concrete beams with macro-synthetic fibres. *Constr. Build. Mater.* 169, 888–899. https://doi.org/10.1016/j.conbuildmat.2018.02.023.
29. Picazo, A.; Gálvez, J.; Alberti, M.; Enfedaque, A. (2018) Assessment of the shear behaviour of polyolefin fibre reinforced concrete and verification by means of digital image correlation. *Constr. Build. Mat.* 181, 565–578. https://doi.org/10.1016/j.conbuildmat.2018.05.235.
30. Picazo, A.; Alberti, M.; Gálvez, J.; Enfedaque, A. (2021) Shear slip post-cracking behaviour of polyolefin and steel fibre reinforced concrete. *Constr. Build. Mater.* 290, 123187. https://doi.org/10.1016/j.conbuildmat.2021.123187.
31. Cendón, D.; Gálvez, J.; Elices, M.; Planas, J. (2000) Modelling the fracture of concrete under mixed loading. *Int. J. Fracture.* 103 [3], 293–310. https://doi.org/10.1023/A:1007687025575.
32. García-Álvarez, V.O.; Gettu, R.; Carol, I. (2000) Numerical analysis of mixed mode fracture in concrete using interface elements, in: Proceedings of the european congress on computational methods in applied sciences and engineering. Barcelona, Spain, pp. 11–14.
33. Suárez, F.; Gálvez, J.; Cendón, D. (2019) A material model to reproduce mixed-mode fracture in concrete. *Fatigue Fract. Eng. M.* 42 [1], 223–238. https://doi.org/10.1111/ffe.12898.
34. ASTM, C. 496-96 (1996) Standard test method for splitting tensile strength of cylindrical concrete specimens.

35. UNE-EN 13279-2. (2014) Gypsum binders and gypsum plasters – Part 2: Test methods.
36. UNE-EN 13279-1. (2009) Gypsum binders and gypsum plasters – Part 1: Definitions and requirements.
37. Suárez Guerra, F.; Felipe-Sesé, L.; Díaz, F.; Gálvez Ruiz, J.; García Alberti, M. (2019) Comportamiento en fractura de yeso con adición de fibras poliméricas. Secretaría del grupo español de la fractura. *Anal. Mecán. Fract*. 36, 114–119.
38. Mayo-Corrochano, C.; Sánchez-Aparicio, L.J.; Aira, J.R., Sanz-Arauz, D.; Moreno, E.; Pinilla Melo, J. (2022) Assessment of the elastic properties of high-fired gypsum using the digital image correlation method. *Constr. Build. Mat.* 317, 125945. https://doi.org/10.1016/j.conbuildmat.2021.125945.
39. C.S. Vic-2D. (2009) Reference manual.
40. Bocca, P.; Carpinteri, A.; Valente, S. (1991) Mixed mode fracture of concrete. *Int. J. Solids Struct.* 27 [9], 1139–1153. https://doi.org/10.1016/0020-7683(91)90115-V.
41. Alonso Vera, J.A. (2015) Estudio de la fisuración en particiones verticales de yeso laminado, producidas por la deformación de forjados. Ph.D. thesis, E.T.S.I. Caminos, Canales y Puertos, (UPM), Madrid.